Thermodynamic Analysis of a GT-sCO_2-ORC-VARS Integrated CCHP System with Solar Energy as Heat Source

Krishna Mani Mishra
Harcourt Butler Technical University, Kanpur (U.P.)

Singh, Onkar
VMSB Uttarakhand Technical University, Dehradun (Uttarakhand)

https://doi.org/10.5109/7236835

出版情報：Evergreen. 11 (3), pp.1834-1847, 2024-09. 九州大学グリーンテクノロジー研究教育センター
バージョン：

Thermodynamic Analysis of a GT-sCO$_2$-ORC-VARS Integrated CCHP System with Solar Energy as Heat Source

Krishna Mani Mishra[1,*], Onkar Singh[2]

[1]Harcourt Butler Technical University, Kanpur (U.P.), India

[2]VMSB Uttarakhand Technical University, Dehradun (Uttarakhand), India

*Author to whom correspondence should be addressed:

E-mail: halkmmishra@gmail.com

(Received July 28, 2023: Revised June 19, 2024: Accepted July 6, 2024).

Abstract: The parametric analysis of combined system having gas turbine, supercritical carbon dioxide (sCO$_2$) Brayton cycle, organic Rankine cycle for power and cooling by vapor absorption refrigeration are studied here. The results provide valuable insights into the exergetic efficiency, exergy destruction, power output, efficiency and refrigeration effect. The combined system offers the maximum exergetic efficiency of 42% at cycle pressure ratio 14, turbine inlet temperature 1400 K, while at these operating states, the power output is 484.38 kW. The variables cycle pressure ratio, turbine intake temperature, and evaporative temperature have all been analyzed for their impact. The GT-sCO$_2$-ORC cycle's power output goes up from 250.53 kW to 484.38 kW and its efficiency goes up from 45.68% to 54.59%, when the cycle's pressure ratio is adjusted from 6 to 14. Maximum exergy destruction of 26% is found in condenser of ORC cycle and negligible in pump. The results of the study demonstrate that, under conditions of 55-60%, LiBr concentration, the coefficient of performance and refrigeration effect of the system exhibit improvement as the generator & evaporator temperature increases. The coefficient of performance and refrigeration effect reach their minimum values i.e. 0.702 and 283.91 kW, respectively at an evaporator temperature of 5°C, whereas their maximum values i.e. 0.775 and 313.39 kW respectively are seen at an evaporator temperature of 15°C.

Keywords: Turbine Inlet Temperature; Exergetic efficiency; Coefficient of performance; Supercritical CO$_2$

1. Introduction

Energy, resources, environment, and human life are all seriously threatened by global warming brought on by excessive carbon emissions[1–8]. As a result, every country on the planet is worried about global warming and attempting to develop a low-carbon, ecologically sound plan of action.[9-11]. The Paris Agreement states that preindustrial levels of warming should not be exceeded by more than 2 °C, with 1.5°C being the optimum[12–14]. In order to reach carbon balance by the middle of this century, countries are making major plans for decarbonized, energy-efficient, and extremely sustainable energy systems[15-17]. In actuality, roughly 50% of worldwide ultimate energy usage comes from heat energy[18–20]. Thermodynamic energy is significant and extensively employed. Recent studies have emphasized the importance of thermal energy in lowering pollution, and examples include the European Road Map for Heat[21–23]. With a rate of 4.3 x 10^{20} J/h, the energy of the sun's rays hitting Earth's surface is about similar to that of 5 million tonnes of unburned coal[24,25]. However, thermal energy continues to be challenging to harness effectively. Around the world, there are an increasing number of sun power projects, and new solar thermal power generation methods and designs are constantly being developed. The organic Rankine cycle (ORC) and heat transfer oil have found extensive usage in places with low and moderate temperatures[26,27]. But many organic fluids that have strong thermodynamic properties also undergo thermal disintegration at high temperatures. The turbine inlet temperature further restricts the potential to increase thermal efficiency. In light of this, conventional steam Rankine cycles and enormous solar tower power plants are still valued[28] and molten salt thermal storage technology is advancing quickly alongside them[29,30]. As a turbine, M. Sharma et al.[31] used an expander with an input temperature of 150 °C. In their environmentally friendly studies, P. Animest et al. used carbon dioxide as a medium [32]. Even though liquid salt is solely utilized as a thermal storage medium, its flaws—including cavitation,

corrosion, uneven heat transmission, thermal insulation, and others—continue to challenge researchers.[33]. The $_sCO_2$ Brayton cycle has experienced fast growth recently[34], and because of its high heat efficiency and tiny engine capacity, it is the most optimistic replace cycle[35,36]. This has made solar energy study into this field very common[37-40]. In order to maximize heat performance, researchers have looked into combining the $_sCO_2$ Brayton cycle with an ORC device[41,42].

Rahman et al. created a portable solar cooling system utilizing a vapor absorption refrigeration system with a LiBr and water combination as an option, capable of cooling 300W[43]. By modelling and developing a solar chiller, Muneer et al. were able to assess the system's efficacy, COP, cooled water temperature, and systems with different types of solar collectors[44]. Choosing an optimal sun collection for the thermal load of the engine Li et al. investigated optimal operation of the device[45]. M.I. Alhamid et al.[46] also investigated the efficiency of cooling towers for machinery, namely condenser components, when used as a coolant to liquify working fluid. This setup is compatible with the same working fluids used and tested by M.A. Islam et al.[58]

Sokhansefat et al. determined the impact of the absorption chiller's solar component on a number of elements, including the collecting field, the temperature set point, and the mass flow rate, and discovered that the current design could use a 28% improvement in efficiency[47].

Thermal energy storage innovations like Heat Transfer Fluid (HTF) and Phase Change Material (PCM) were mentioned as examples of the technical advances made by the different parts of the solar-powered combined cycle system.[48-52]. Using intercooling and warming of the gas engine, researchers performed temperature study of the integrated combined cycle[53]. Researchers analysed the impacts of heat recovery steam generators, intake misting, and steam input on combined cycles, and assessed how these factors affect power facilities[54,55].

2. Objective/Novelty of Present Study

After the literature survey, there appears to further utilize available energy in waste heat in an integrated GT-sCO_2- ORC-VARS system. Present work deals with the thermodynamic modeling and analysis of a solar powered combined power cycle consisting of the Brayton cycle, supercritical CO_2 and Organic Rankine cycle along with VARS based on first law and the second law of thermodynamics.

Therefore, the present combined arrangement is studied for utilizing the waste heat to run the VARS based on LiBr-H_2O while using the exhaust heat in HRVG for powering organic Rankine cycle to augment the power output. The potential of the proposed combined power & cooling system is thermodynamically investigated through the First & Second law of thermodynamics study of integrated system. The ORC used for utilizing the waste heat runs on the working fluid R152a for getting the expansion work from the ORC turbine. For effective heat utilisation, it is clear that more study on solarized integrated cycles using air/sCO_2 as the working fluid and integrating them with organic Rankine cycles and other low temperature power cycles is warranted. Parabolic collectors are widely used to recover solar energy, but heliostat-based systems perform better, making them an appealing choice for solar energy capture[68]. This approach is applied in the current investigation with continuous sun irradiation. As of best of author's knowledge, an innovative GT- sCO_2-ORC and Cooling cycle combination has not been studied from this perspective and hence same has been suggested to accomplish the following objectives:

- To perform parametric analysis of integrated systems
- To study the effect of gas turbine inlet temperature, pressure ratio on the cycle performance like efficiency, power output etc.
- Examine the effect of evaporation temperature on Refrigeration Effect & COP of VARS.
- To calculate Exergetic Efficiency in Different Cycle Combination.
- To determine the exergy destroyed by each constituent

3. System Description

Schematic diagram of the GT-sCO_2-ORC-VARS Integrated System has been shown in the Fig.1. Here, air is compressed in GT cycle and exhaust of GT is used as input to sCO_2 cycle, which is combined with ORC cycle. Exhaust from WHB is used to get the cooling effect from VARS cycle. R152a is used as ORC fluid while LiBr-H_2O combination is used for cooling cycle. Air enters at air compressor at state 1 and takes heat from molten salt solution between state 2 and state 3 while molten salt has been heated through solar heliostat from state a to state b. Then, air is expended in turbine from state 3 to state 4 and rejected to waste heat boiler from state 4 to 5. In waste heat boiler, the heat is grabbed by sCO_2 fluid between state 8 to state 9 coming from sCO_2 compressor at state 8. Then, sco2 fluid enters the sCO_2 -turbine. Then, reject heat in heat exchanger of sCO_2 from state 9 to state 10. The heat rejected from sCO_2 fluid between state 10 and state 7 is consumed by ORC fluid between state 12 and state 13coming from ORC-pump at state 11. Then, ORC fluid is used at the turbine between states 13 and 14 and condensed from water between states 14 and 11 between states 16 and 17. The exhaust air coming from state 5 is used to heat generator temperature of LiBr-H_2O solution at state 17 and state 24 in VARS cycle. The steam only passes through condenser at state 17 and rest LiBr-H_2O solution returned to heat exchanger at state 24 and absorber at state 25 and state 26. The H_2O refrigerant is condensed in condenser from state 17 and state 18 and

then expansion takes place through throttling valve between state 18 and state 19. Then, at state 19, the refrigerant enters the absorber, where it absorbs heat before returning to condition 19. The absorber uses heat to bring about the desired concentration ratio in the LiBr-H_2O combination. The LiBr-H_2O combination is moved from state 21 to 22, where it is heated by a heat exchanger before entering state 23 and finally powering a generator. The exhaust air finally is relieved into atmosphere at state 6. In the current analysis, a mixture of LiCl (59.5%) and KCl (49.5%) is used as molten salt.The thermophysical properties along with input parameters are mentioned in in Table 1.

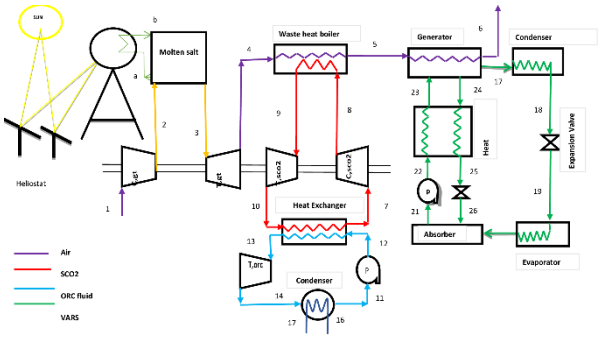

Fig. 1. Schematic diagram of the GT-sCO$_2$-ORC-VARS Integrated System

Table 1: Input Parameters

Parameters	Value	Ref.
Total Heliostat aperture area	10,000 m^2	56
Heliostat efficiency	75 %	56
Solar Irradiation	1000 W/m^2	56
Receiver efficiency	80 %	56
Molten Salt heat exchanger effectiveness	95 %	56
Boiling temperature of Molten salt	1400°C	56
Melting temperature of Molten salt	354°C	56
heliostat field temperature	1500°C	56
Polytropic efficiency of compressor	90%	57
Inlet temperature	298 K	58
Polytropic efficiency of turbine	92%	57
Effectiveness of waste heat recovery boiler	0.85	57
Temperature at inlet of sCO$_2$ compressor	304 K	62
sCO$_2$ compressor inlet pressure	7.2 MPa	62
CPR of sCO$_2$ cycle	2.8	62
sCO$_2$ turbine's isentropic efficiency	90%	62
sCO$_2$compressor's isentropic efficiency	89%	62
Critical temperature for sCO$_2$	30.97°C	59
Critical pressure for sCO$_2$	7.3773 MPa	59
R152a turbine inlet temperature	373 K	63
R152a turbine inlet pressure	20.429 bar	63
R152a turbine outlet pressure	3.7 bar	63
R152a condenser outlet temperature	283 K	63
Critical temperature for R152a	113.5°C	59
Critical pressure for R152a	4.58 MPa	59
ORC turbine isentropic Efficiency	90%	63
Initial percentage of LiBr in solution	55 %	60
Final percentage of LiBr in solution	60 %	60
Generator Temperature	363 K	60
Condenser Temperature	323 K	60
Evaporator Temperature	288 k	60
Absorber Temperature	313 K	60
Dead state Temperature	298 K	60

4. Assumptions

The thermodynamic modelling of the under-consideration cycle configuration takes the following presumptions into account:

- The heat exchanger, pump, compressor, and turbines are all operating in line with the necessary thermodynamic processes, and varied efficiencies as indicated in the input parameters are used to make up for non-ideal operation.
- Each part of the system experiences insignificant shifts in the kinetic and potential exergy terms.
- There is no change in either the temperature or pressure of the surrounding environment (To = 298 K, Po = 100 kPa).
- If air were a perfect atmosphere, its 21% oxygen and 79% nitrogen molar makeup would be calculated.
- The solution is at saturated state when coming out of the absorber and generator, and the refrigerant is at saturated state when leaving the condenser and evaporator.
- The generator and condenser pressure are equivalent, whereas the absorption and evaporator pressure are equivalent.
- No pressure drops due to friction in the pipe.

5. Mathematical Modelling

The following statements from the first and second laws of thermodynamics form the basis for the analysis presented here:

$$Ex = (h-h_0) - T(S-S_0) \quad (1)$$

Following equations are shown for the different cycles and their components:

5.1 Gas turbine cycle

a. Compressor

$$\frac{T_2}{T_1} = \left(\frac{P_2}{P_1}\right)^{\left(\frac{\gamma-1}{\gamma \times \eta_{P,comp}}\right)} \quad (2)$$

Power requirement in compressor is,

$$Wcomp = m_1 (h_2-h_1) \quad (3)$$

Exergy destruction in compressor is,

$$Excomp = m_1(Ex_1-Ex_2) \quad (4)$$

Heat gained by air in a molten salt heat exchanger in kW is given as ,

$$Qair = \int_{T2}^{T3} ma \cdot cp(T)dT \quad (4.1)$$

b. Turbine

Expansion pressure and temperature are linked by,

$$\frac{T_3}{T_4} = \left(\frac{P_3}{P_4}\right)^{\left(\frac{\gamma-1}{\gamma}\right)*\eta_{P,tur}} \quad (5)$$

Humid air turbine's power output is:

$$Wtur = m_1 (h_3-h_4) \quad (6)$$

Exergy destruction in turbine is,

$$Extur = m_1(Ex_3-Ex_4) \quad (7)$$

c. Waste heat boiler

$$Q_{whb} = m_1(h_4-h_5) = m_8(h_9-h_8) \quad (8)$$

Exergy destruction in waste heat boiler is,

$$Exwhb = m_1(Ex_4-Ex_5)-m_{sco2}(Ex_9-Ex_8) \quad (9)$$

Power output of the GT cycle is,

$$W_{GT,net} = W_{GT,tur} - W_{GT,comp} \quad (10)$$

Total exergetic destruction of GT system is,

$$Exd_{total,GT} = Exd_{tur} + Exd_{comp} + Exd_{HX} + Exd_{whb} \quad (11)$$

Efficiency of GT cycle,

$$\eta_{GT} = \frac{W_{GT,net}}{Q_{HX}} \quad (12)$$

The exergetic efficiency of the GT system is,

$$\eta_{exergetic,GT} = 1 - \frac{Exd_{total,GT}}{W_{GT,net}} \quad (13)$$

5.2 Supercritical Carbon Dioxide Cycle

Output from sCO_2 turbine:

$$W_{SCO2,tur} = m_{SCO2}(h_9-h_{10}) \quad (14)$$

Exergy destruction in sCO_2 turbine is,

$$Ex_{SCO2,tur} = m_{sco2}(Ex_9-Ex_{10}) \quad (15)$$

Heat exchanger:

$$Q_{SCO2,heat\ exchanger} = m_{SCO2}(h_{10}-h_7) \quad (16)$$

Exergy destruction in heat exchanger is,

$$Ex_{SCO2,heat\ exchanger} = m_{sco2}(Ex_{10}-Ex_7)-m_{ORC}(Ex_{13}-Ex_{12}) \quad (17)$$

Power requirement in sCO_2 compressor:

$$W_{SCO2,comp} = m_{SCO2}(h_8-h_7) \quad (18)$$

Exergy destruction in sCO_2 compressor is,

$$Ex_{SCO2,comp} = m_{sco2}(Ex_8-Ex_7) \quad (19)$$

Power output of the sCO_2cycle is,

$$W_{SCO2,net} = W_{SCO2,tur} - W_{SCO2,comp} \quad (20)$$

Efficiency of sCO_2cycle,

$$\eta_{SCO2} = \frac{W_{SCO2,net}}{Q_{whb}} \quad (21)$$

Total exergetic destruction of sCO_2 system is,

$$Exd_{total,sCO2} = Exd_{SCO2,tur} + Exd_{SCO2,whb} + Exd_{SCO2,heat\ exchanger} + Exd_{SCO2,comp} \quad (22)$$

The exergetic efficiency of the sCO_2 system is,

$$\eta_{exergetic,GT} = 1 - \frac{Exd_{total,sco2}}{W_{sco2,net}} \quad (23)$$

5.3 Organic Rankine Cycle

The following is the heat balance calculation for ORC heat exchanger:

$$Q_{sco2,HE} = m_{SCO2}(h_{10}-h_7) = m_{ORC}(h_{13}-h_{12}) \quad (24)$$

Power produced in the ORC turbine:

$$W_{ORC,tur} = m_{ORC}(h_{14}-h_{11}) \quad (25)$$

Exergy destruction in ORC turbine is,

$$Ex_{ORC,tur} = m_{ORC}(Ex_{14}-Ex_{11}) \quad (26)$$

Heat rejection in the condenser:

$$Q_{ORC,cond} = m_{ORC}(h_{37}-h_{38}) \quad (27)$$

Exergy destruction in heat exchanger is,

$$Ex_{ORC,heat\ exchanger} = m_{ORC}(Ex_{14}-Ex_{11})-m_{water}(Ex_{17}-Ex_{16}) \quad (28)$$

Power requirement in the ORC pump:

$$W_{ORC,pump} = m_{ORC}(h_{12}-h_{11}) \quad (29)$$

Exergy destruction in ORC pump is,

$$Ex_{ORC,pump} = m_{ORC}(Ex_{12}-Ex_{11}) \quad (30)$$

The power output of the ORC system is,

$$W_{ORC,net} = W_{ORC,tur} - W_{ORC,pump} \quad (31)$$

The efficiency of the ORC system is,

$$\eta_{ORC} = \frac{W_{ORC,net}}{Q_{sco2.heat\ exxhanger}} \quad (32)$$

Total exergetic destruction of ORC system is,

$$Exd_{total,ORC} = Exd_{tur} + Exd_{cond} + Exd_{heat\ exchanger} + Exd_{pump} \quad (33)$$

The exergetic efficiency of the ORC system is,

$$\eta_{exergetic,ORC} = 1 - \frac{Exd_{total,ORC}}{W_{ORC,net}} \quad (34)$$

5.4 Vapour Absorption Refrigeration System

a. Generator

The energy balance of the machine can be written as

$$Q_{gen} = m_{17}h_{17} + m_{24}h_{24} - m_{23}h_{23} \quad (35)$$

Exergetic destruction is expressed as

$$Exd_{gen} = m_{17}Ex_{17} + m_{24}Ex_{24} - m_{23}Ex_{23} \quad (36)$$

b. Condenser

The condenser's energy balance is given by

$$Q_{con} = m_{17}h_{17} - m_{18}h_{18} \quad (37)$$

Exergetic destruction is expressed as

$$Exd_{con} = m_{17}Ex_{17} - m_{18}Ex_{18} \quad (38)$$

c. Evaporator

The evaporator's mass and energy balance results in the following.

$$\text{Refrigerant effect} = Q_{eva} = m_{19}(h_{20} - h_{19}) \quad (40)$$

Exergetic destruction is expressed as

$$Exd_{eva} = m_{19}(Ex_{20} - Ex_{19}) \quad (41)$$

d. Absorber

When water vapour of low pressure and low temperature mixes with LiBr strong solution inside the absorber, an exothermic reaction occurs. The absorber energy balance equation is shown below:

$$Q_{abs} = m_{20}h_{20} + m_{26}h_{26} - m_{21}h_{21} \quad (42)$$

Exergetic destruction is expressed as

$$Exd_{abs} = m_{20}Ex_{20} + m_{26}Ex_{26} - m_{21}Ex_{21} \quad (43)$$

The performance coefficient is abbreviated

$$COP. = \frac{R.E.}{Q_{gen}} \quad (44)$$

The exergetic efficiency is,

$$\eta_{exergetic,VARS} = \frac{Q_{eva}\left(1 - \frac{T_o}{T_{eva}}\right)}{Q_{gen}\left(1 - \frac{T_o}{T_{gen}}\right) + W_{pump}} \quad (45)$$

Total exergetic destruction is,

$$Exd_{total,VARS} = Exd_{eva} + Exd_{con} + Exd_{gen} + Exd_{abs} \quad (46)$$

Following performance evaluation factors are also evaluated in the present study:

$$\text{Total Power} = W\_net = W_{GT,net} + W_{SCO2,net} + W_{ORC,net} \quad (47)$$

$$\text{Heating} = \text{heating across ORC condenser} \quad (48)$$

$$\text{Cooling effect} = \text{Refrigerant effect} \quad (49)$$

Flow chart has been included regarding calculation/simulation techniques. Same is shown in Fig.2, below:

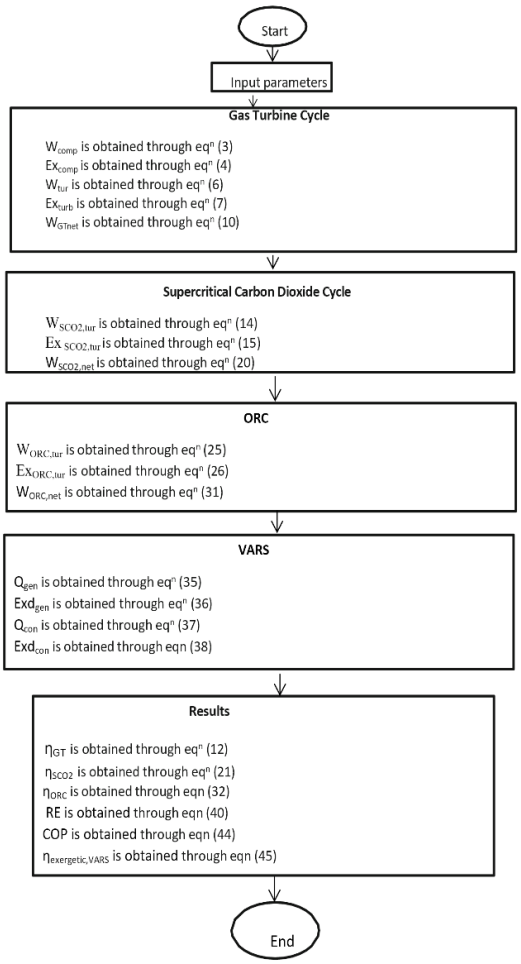

Fig.2. Flow chart showing mathematical model of the research undertaken

6. Results & Discussions

In this part, thermodynamic modelling and exergy analysis of integrated systems with varying input parameters have been presented. Thermodynamic properties i.e. enthalpy, pressure, temperature, entropy, mass flow rates etc. are tabulated in Table 2. Refprop7[65] and EES-software[66] are used for the enthalpy calculation and mathematical modeling of the combined system respectively. Results obtained for different parametric variations have been plotted graphically and analyzed suitably.

6.1 Impact of Cycle Pressure Ratio (CPR) on Power output & Energy Efficiency of GT Cycle

Figure 3 depicts the impact of CPR on the power output and efficiency of the GT cycle as it changes from 6 to 14. Graph shows that the power output increases as the CPR increases. The air temperature rises at the end of the compression process as the cycle pressure ratio increases, which raises the turbine inlet temperature for the available heat from solar radiation. Reduced gas turbine exit temperature and increased gas turbine work production are caused by an increase in cycle pressure ratio.

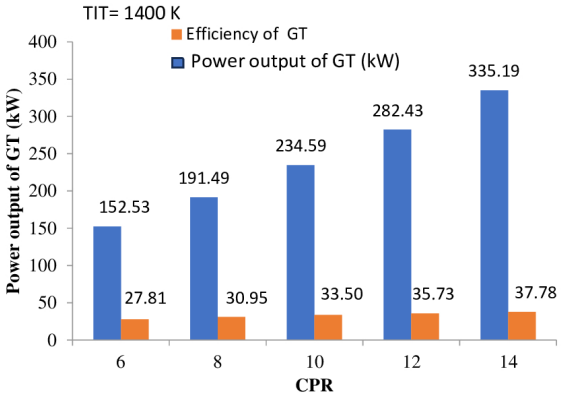

Fig. 3. Impact of Cycle Pressure Ratio (CPR) on Power output & Energy Efficiency of GT Cycle

6.2 Impact of Cycle Pressure Ratio (CPR) on Power output & Efficiency of GT- sCO_2 Cycle

The increase in efficiency and the decrease in power output of the GT-sCO_2 cycle from a pressure ratio of 6 to 14 are shown in Fig. 4. Graph is plotted at TIT= 1400 K, CPRsco2 = 2.83, $T_{cond,sco2}$ = 304 K, Ttur,sco2 =542 K. According to the graph, the power output of the GT-sCO_2 cycle increases from 213.61 kW to 428.16 kW as the CPR of GT increases from 6 to 14. The efficiency & power output of the cycle increases as cycle pressure ratio is increased. In order to get a higher turbine intake temperature for the available solar radiation heat, the cycle pressure ratio must be increased since doing so raises the temperature of the air at the conclusion of the compression phase. By raising the cycle pressure ratio, the temperature of the air at the conclusion of the compression process rises, resulting in a greater turbine inlet temperature for the solar radiation heat that is available and rise in the pressure ratio of the cycle, coupled with the constant availability of solar radiation heat, results in a decrease in the temperature at which the gas turbine exhausts, thus leading to an increase in the power output of the gas turbine. However, the power output of the sCO_2 turbine will be impacted because of the decrease in energy available in the waste heat boiler (WHB) as a result of the lower gas turbine exit temperature. But overall power output increases for combined GT- sCO_2 cycle with increase of CPR. Increasing the CPR of the GT from 6 to 14 increases the efficiency of the combined GT- sCO_2 cycle from 38.95% to 48.25%, but beyond a certain point, the efficiency decreases because increasing the CPR lowers the gas turbine exit temperature, which in turn increases the gas turbine power output. However, the efficiency of the sCO_2 turbine will suffer as a result of the decrease in energy available in the waste heat boiler (WHB) due to the lower gas turbine exit temperature. But overall efficiency increases for combined GT- sCO_2 cycle with increase of CPR.

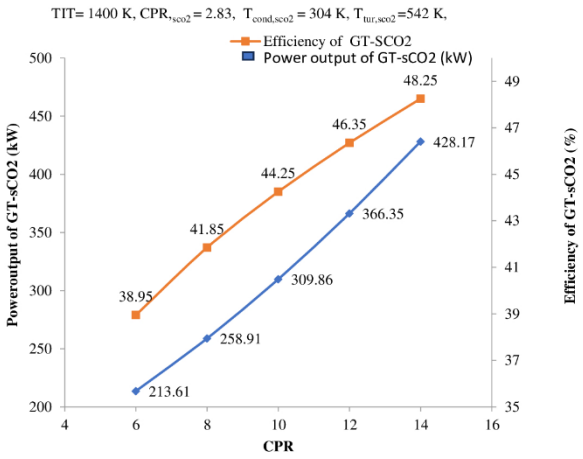

Fig. 4. Impact of Cycle Pressure Ratio (CPR) on Power output & Efficiency of GT- sCO_2 Cycle

6.3 Impact of Cycle Pressure Ratio (CPR) on Power output & Efficiency of GT-SCO_2-ORC system

Figure 5 indicates power output and efficiency of the GT-sCO_2-ORC cycle at TIT= 1400 K, $CPR_{,sco2}$ = 2.83, $CPR_{,ORC}$ = 5.52. $T_{cond,sCO2}$ = 304 K, $T_{tur,sco2}$ =542 K, $T_{tur,ORC}$=373. Graph shows that as CPR of GT goes from 6 to 14, the output of GT cycle goes up from 250.53 kW to 484.38 kW. The increase in GT-sCO_2-ORC power output & energy efficiency with cycle pressure ratio is responsible for the cycle's overall increase in power output. The air temperature rises at the end of the compression process as the cycle pressure ratio increases, which raises the turbine inlet temperature for the heat from available solar radiation. Reduced gas turbine exit temperature and increased gas turbine work production are caused by an increase in cycle pressure ratio and the availability of the same quantity of solar radiation heat. However, because the sCO_2 and ORC turbines rely on the energy available in the WHB, the fall in gas turbine exit temperature will have a negative impact on their productivity. However, for the combined GT- sCO_2-ORC cycle, the total amount of effort increases as CPR rises. Further, efficiency graph shows that as CPR of GT increases from 6 to 14, efficiency of combined GT- sCO_2-ORC cycle rises from 45.68 % to 54.59 %. However, efficiency decreases after a certain point because increasing CPR decreases gas turbine exit temperature and, in turn, increases gas turbine power output. However, the efficiency of the sCO_2 turbine will suffer as a result of

the decrease in energy available in theWHB due to the lower gas turbine exit temperature. But overall efficiency increases for combined GT- sCO_2 cycle with increase of CPR.

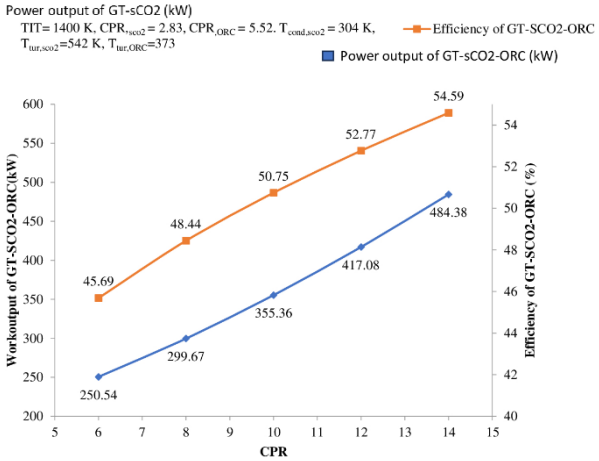

Fig. 5. Impact of Cycle Pressure Ratio (CPR) on Power output & Efficiency of GT-sCO_2-ORC System

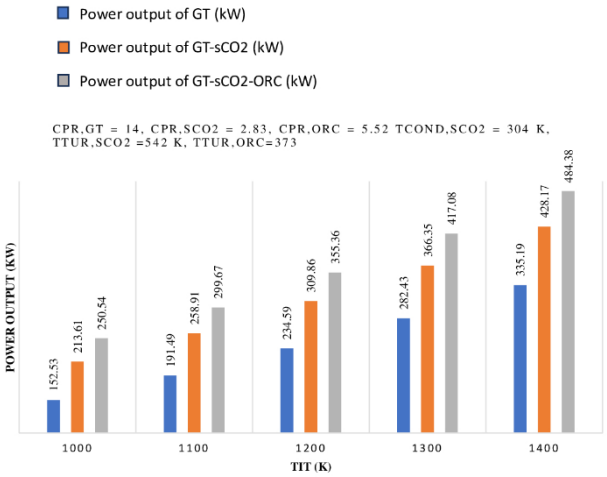

Fig. 6. Impact of TIT on Power output of GT, GT-sCO_2 & GT-sCO_2-ORC

6.4 Impact of TIT on Power output of GT, GT-sCO_2 & GT-sCO_2-ORC

In the system under investigation, the TIT is also an important control parameter. Figure 6 depicts the effect of changing the TIT of the gas turbine from 1000 K to 1400 K at $CPR_{,GT}$ = 14, $CPR_{,sco2}$ = 2.83, $CPR_{,ORC}$ = 5.52. $T_{cond,sco2}$ = 304 K, $Ttur_{,sco2}$ =542 K, $T_{tur,ORC}$=373 on the work production of the GT, GT-sCO_2, and GT-sCO_2-ORC cycles. Work production rises for GT cycle varies from 152.53 kW to 335.19 kW, for GT-sCO_2 varies from 213.61 kW to 428.17 kW and for GT-SCO_2-ORC varies from 250.54 kW to 484.38 kW as TIT increases from 1000 K to 1400 K. By raising the temperature at which the turbine receives the incoming air, we can improve the efficiency of converting energy. Increased temperature facilitates enhanced heat transfer, leading to a higher magnitude of heat energy being conveyed to the turbine blades. Consequently, this results in heightened power generation and enhanced overall efficiency of the gas turbine. As the TIT was raised, the net work production of the GT-based combined system rose. The enthalpy of the gases increases as the TIT rises. The specific heat of gases increases with temperature. As a consequence, the amount of work produced by the gas turbine increases at the same mass flow rate. The efficiency and sustained net power output of a gas turbine combined system operating at a high pressure ratio are both enhanced by a high TIT. High TIT might be difficult to generate due to metallurgical limitations. The turbine's blades begin to break at high temperatures, reducing its durability and life span.

6.5 Impact of TIT on Efficiency of GT, GT-sCO_2 & GT-SCO_2-ORC systems

Figure 7 demonstrates how the efficiency of the GT, GT-sCO_2, and GT-sCO_2-ORC cycles changes when the temperature in the cycle is adjusted. Graph depicts the effect of changing the TIT of the gas turbine from 1000 K to 1400 K at $CPR_{,GT}$ = 14, $CPR_{,sco2}$ = 2.83, $CPR_{,ORC}$ = 5.52. $T_{cond,sco2}$ = 304 K, $T_{tur,sco2}$ =542 K, $T_{tur,ORC}$=373 on the work production of the GT, GT-sCO_2, and GT-sCO_2-ORC cycles. Efficiency rises for GT cycle varies from 27.81% to 37.78%, for GT-sCO_2 varies from 38.95 % to 48.25 % and for GT-sCO_2-ORC varies from 45.69 % to 54.59 % as TIT increases from 1000 K to 1400 K. Altering the TIT from 1000 K to 1400 K results in commensurate performance adjustments. From TIT 1000 K to TIT 1400 K, there is a 10.48%-11.14% effectiveness difference due to the incorporation of the sCO_2 cycle into the GT cycle. When the ORC cycle is included in the GT-sCO_2 cycle, the efficiency shifts from 6.33 percent to 6.73 percent between TIT 1000 K and TIT 1400 K. By raising the temperature at which the turbine receives the incoming air, we can improve the efficiency of converting energy. Increased temperature facilitates enhanced heat transfer, leading to a higher magnitude of heat energy being conveyed to the turbine blades. Consequently, this results in heightened power generation and enhanced overall efficiency of the gas turbine.

Table 2: Fluid states in combined GT-sCO$_2$-ORC-VARS system for typical CPR of 8 and TIT of 1100 K

State Point	P (bar)	T (K)	m (kg/s)	h (kj/kg)	S (kj/kgK)	Ex (kj)
1	1	300	1	426.04	3.8881	0.22
2	8	580.91	1	713.08	3.9642	263.99
3	8	1100	1	1287.9	4.6674	627.85
4	1	696	1	835.27	4.7538	149.3
5	1	373	1	499.67	4.1078	7.5
6	1	343	1	469.37	4.0231	2.61
7	72	304	1.22	384.56	1.6075	642.48
8	204	373	1.22	423.62	1.6257	676.08
9	204	542	1.22	687.46	2.2202	761.57
10	72	434	1.22	598.35	2.2176	673.24
11	3.7	282	0.8585	216.8	1.06	638.97
12	20.42	283	0.8585	217.45	1.056	640.82
13	20.42	373	0.8585	587.33	2.1534	681.48
14	3.7	301	0.8585	534.35	2.1802	620.46
17	0.12	363	0.0123	2668.1	8.3008	918.03
18	0.12	323	0.0123	209.34	0.7038	738.36
19	0.017	288	0.0123	209.34	0.7324	729.76
20	0.017	288	0.0123	2528.2	8.7815	633.92
21	0.017	313	0.1481	94.39	0.2456	760.88
22	0.123	313	0.14811	98.45	0.2585	761.07
23	0.123	338	0.14811	145.7	0.4034	764.85
24	0.123	363	0.13577	214.1	0.5073	802.08
25	0.123	338	0.13577	165.5	0.3688	795.03
26	0.017	313	0.13577	117.9	0.2225	791.32

As the TIT was raised, the net work production of the GT-based combined system rose. The efficiency and sustained net power output of a gas turbine combined system operating at a high pressure ratio are both enhanced by a high TIT. High TIT might be difficult to generate due to metallurgical limitations.

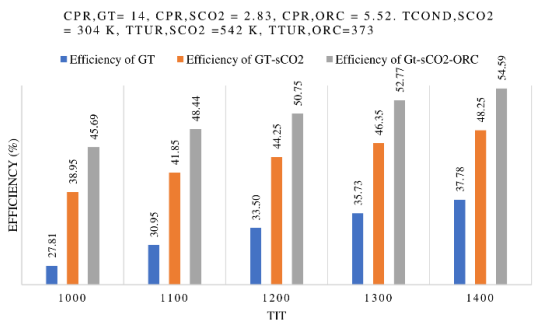

Fig. 7. Impact of TIT on Efficiency of GT, GT-sCO$_2$ & GT-sCO$_2$-ORC Systems

The enthalpy of gases increases as the TIT rises. The specific heat of gases increases with temperature. As a consequence, the amount of work produced by the gas turbine increases at the same mass flow rate.

6.6 Impact of Evaporative Temperature on Refrigeration Effect & COP of VARS

Figure 8 displays the impacts of changing the evaporative temperature on the system's COP and RE for evaporative temperatures between 5°C and 15°C for T5= 373 K, T6= 343 K, Tgen = 363 K, Tabs= 313 K, and Tcond = 323 K. With 55%-60% LiBr concentration, it is shown that the system's COP and RE become better as the evaporator temperature rises. Graphical depiction in Figure 8 shows variation in COP values and RE values at different evaporative temperatures. Raghuvanshi et al. analyzed the LiBr based cooling cycle at 5°C[67]. The increase in evaporator temperature leads to a reduction in the required amount of refrigerant, resulting in higher COP. For the purpose of this study, the pressure in the evaporator and the absorber are being considered as equivalent. A greater evaporator pressure corresponds to a higher absorber pressure, given the same absorber temperature. This enhances the mass output from the

Absorber, thereby reducing the heat load on the Generator and increasing the COP.

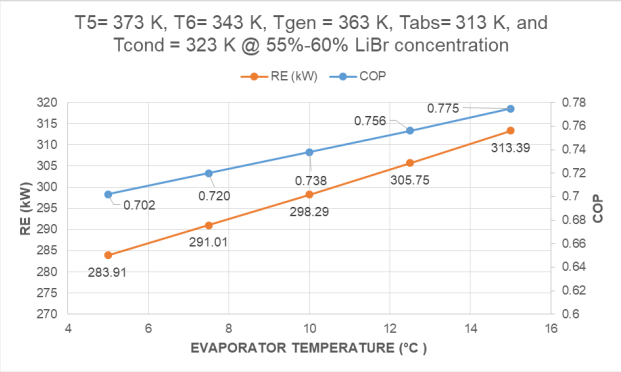

Fig. 8. Impact of Evaporative Temperature on Refrigeration Effect & COP of VARS

6.7 Exergy Destruction in Components of Combined System

Exergy destruction in different components are plotted in pie chart in Fig.9 at TIT= 1400 K, CPR,GT=14, CPR,$_{sCO2}$ = 2.83, CPR,$_{ORC}$ = 5.52. T$_{cond,\ sCO2}$ = 304 K, T$_{tur,sCO2}$ =542 K, T$_{tur,ORC}$=373 K, Tgen =363 K, Tabs= 313 K, Tcond = 323 K. Compressor work, and hence exergy destruction, is observed to rise with increasing cycle pressure ratio.

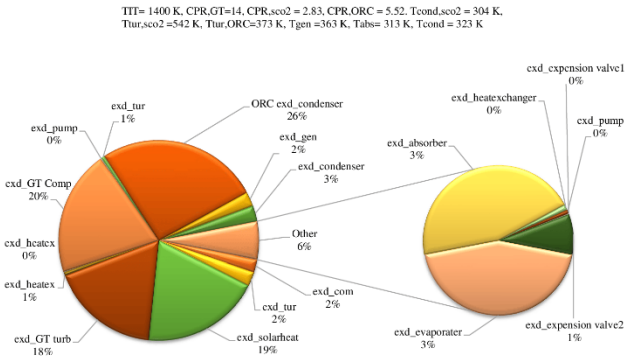

Fig. 9. Exergy destruction in Components of Combined System

The ORC condenser is responsible for the greatest amount of exergy destruction and loss in the cycle at 26%, followed by the GT compressor at 20% and the solar heat exchanger at 19%. That's why it's so important for these parts to function efficiently inside the cycle. If these parts are better designed and made to function together, the cycle's productivity and efficiency will increase. It also means that the effectiveness of these three parts is essential to the cycle's functioning. Heat exchangers, pumps, and expansion valves all have minimal amounts of irreversibility.

6.8 Exergy Destruction in Combined Cycles

Exergy destruction has been shown for the different combination of cycles at TIT= 1400 K, CPR,$_{GT}$=14, CPR,$_{sco2}$ = 2.83, CPR,$_{ORC}$ = 5.52. T$_{cond,sco2}$ = 304 K, T$_{tur,sco2}$ =542 K, T$_{tur,ORC}$=373, Tgen =363 K, Tabs= 313 K, Tcond = 323 K in the Fig. 10. It reveals that the exergy destruction in the VARS system is maximum whereas in the GT cycle it is minimum. As the exergy of the exhaust gas entering the refrigeration cycle rises as a result of an increase in process heat, it has been found that the exergy destruction in all components of the VARS cycle is greater. This causes further loss of refrigerant via the generator. This means that there is a greater exergy degradation in the refrigeration cycle overall. As the process heat rises, it is also seen that the exergy destruction in each part of the vapour absorption refrigeration system rises. There would be a rise in exergy destruction across the board in the vapour absorption system as the mass flow rate of the refrigerant in the generator increased.

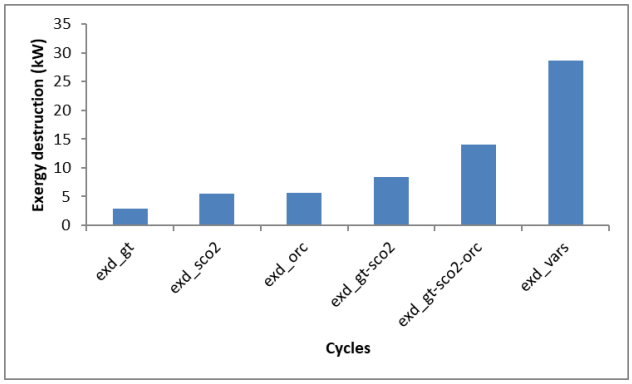

Fig. 10. Exergy Destruction in Combined Cycles

6.9 Exergetic Efficiency in Different Cycle Combination

Exergetic efficiency of the entire combined cycles/CCHP are depicted in Fig.11 at TIT= 1400 K,CPR,$_{GT}$ =14,CPR,$_{sco2}$ = 2.83,CPR,$_{ORC}$ = 5.52, T$_{cond,sco2}$ = 304 K, T$_{tur,sco2}$ =542 K, T$_{tur,ORC}$=373, Tgen =363 K, Tabs= 313 K, Tcond = 323 K . Compared to other parts, the VARS has the greatest exergy efficiency.

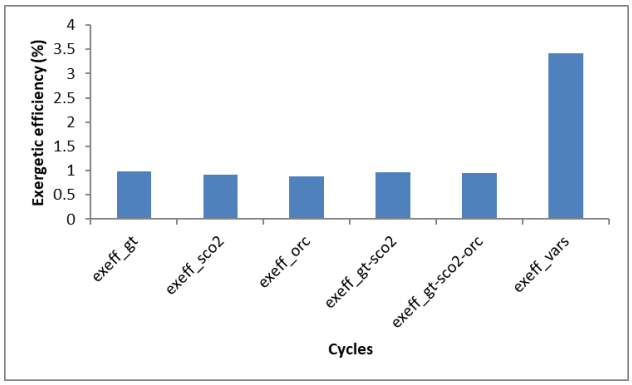

Fig. 11. Exergetic Efficiency in Different Cycle Combination

7. Model Validation

This study is novel, no such work has been done so far as of the best of authors knowledge. Accordingly, validation has been done for different cycles and compared with concerned literature work as as per the best available data and found within permissible limit. Table 3 displays the validation outcomes.

Table 3: Validation

GT Validation			
CPR	**Efficiency of Khalique et al.[61] (%)**	**Efficiency obtained in present work (%)**	**Error diff.**
8	34	30.95	3.05
12	37	35.73	1.27
16	39	38.78	0.22
20	40	39.86	0.14
sCO_2 Validation			
CPR	**Efficiency of Dostal et al. [62] (%)**	**Efficiency obtained in present work (%)**	**Error diff.**
3	39	39.56	0.56
3.5	38.2	38.96	0.76
4	37.4	38.18	0.78
ORC Validation			
Evaporative Temp. (°C)	**Efficiency of Wei et al.[63] (%)**	**Efficiency obtained in present work (%)**	**Error diff.**
55	5.4	6.33	0.93
60	6	7.78	1.78
65	7.3	8.126	0.826
70	8.2	8.339	0.139
VARS Validation			
Generator temp. (°C)	**COP of Kilic et al. [64]**	**COP obtained in Present work**	**% diff.**
80	0.68	0.615	9.56
85	0.72	0.664	7.778
90	0.75	0.708	5.60
95	0.77	0.724	5.97

Validation graphs are given below:

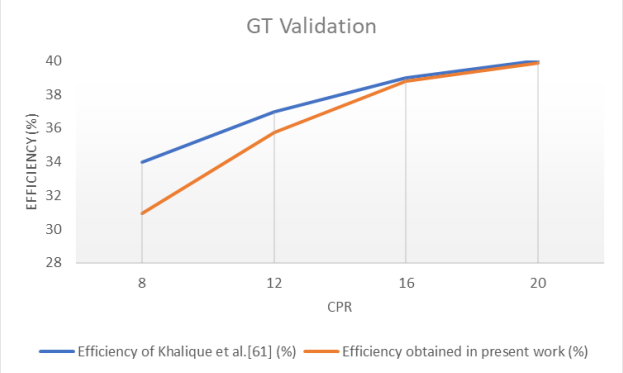

Fig. 12. Validation graph for GT system

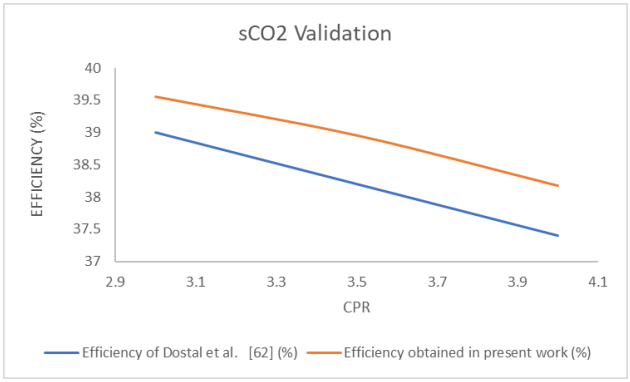

Fig. 13. Validation graph for sCO_2 system

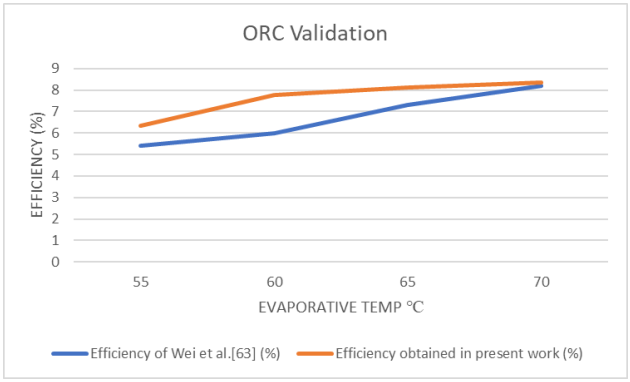

Fig. 14. Validation graph for ORC system

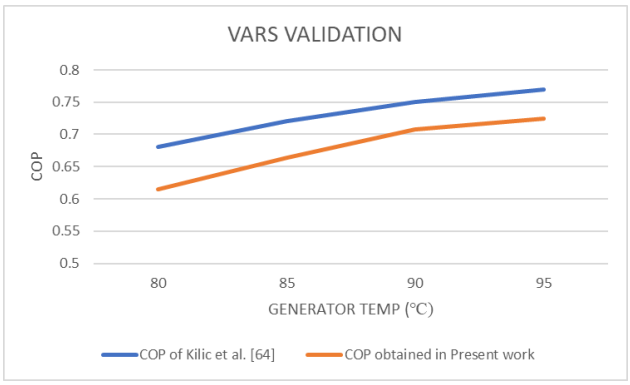

Fig. 15. Validation graph for VARS system

8. Conclusions

The conclusions obtained from a computer-assisted thermodynamic model and investigation of a solar-powered GT-sCO_2-ORC, along with a VARS system, are outlined below:

- The present research demonstrated that the TIT & CPR had a significant impact on power output and efficiency.
- Maximum power output for GT system is 335.18 kW, GT-sCO_2 cycle is 428.16 kW & GT- sCO_2-ORC cycle is 484.38 kW.
- Maximum efficiency for GT- sCO_2-ORC cycle is 54.59% at TIT is 1400 K & CPR is 14.Maximum COP value as 0.707935 and RE as 286.15 kW at evaporative temperature at 15°C .

- Maximum Exergy Destruction (MED) is displayed in the condenser of the ORC cycle and minimal MED is displayed in the pump across a variety of systems, while MED is displayed in the condenser of the VARS cycle and MED is displayed in the condenser of the GT cycle.
- The Maximum Exergetic Efficiency is shown in VARS cycle and minimum is in ORC cycle.
- The total power of the combined system is 272.13 kW, heating across ORC condenser utilized for water heating is 65.22 kW and refrigeration effect is 28.52 kW at CPR of 8 and TIT of 1100 K.

Nomenclature

Symbols

m	Mass flow rate in kg/s
h	Enthalpy in kJ/kg
S	Entropy in kJ/kg K
P	Pressure in bar
ε	Heat exchanger effectiveness
T	Temperature in K
Q	Heat, kW
W	Power, kW
Ƞ	Efficiency
Ex	Exergy
I	Solar Irradiation (W/m^2)
A	Area of Heliostat (m^2)

Abbreviations

GT	Gas turbine
CCHP	Combined Cooling, Heating and Power
sCO$_2$	Supercritical carbon dioxide
ORC	Organic Rankine Cycle
VARS	Vapour Absorption Refrigeration System
R152a	1,1-Difluroethane
LiBr	Lithium bromide
CPR	cycle pressure ratio
TIT	Turbine inlet temperature in K
RE	Refrigerant Effect
COP	Coefficient of performance
MED	Maximum Exergy Destruction

Subscripts

Ƞp	Polytopic Efficiency
η_H	heliostat efficiency
η_R	receiver efficiency
ε_{HX}	heat exchanger effectiveness
comp	Compressor
tur	Turbine
cond	Condenser
net	Net
tot	Total
whb	Waste heat boiler
gen	Generator
eva	Evaporator
abs	Absorber

References

1) Hoedi Prasetyo, "On-grid photovoltaic system power monitoring based on open source and low-cost internet of things platform," Evergreen, 8 (1) 98–106 (2021). doi:10.5109/4372265.
2) Siva Subrahmanyam Mendu, P. Appikonda, and Anil Kumar Emadabathuni, "Techno-economic comparative analysis between grid-connected and stand-alone integrated energy systems for an educational institute," Evergreen, 7 (3) 382–395 (2020). doi:10.5109/4068616.
3) M.K. Barai, and B.B. Saha, "Energy security and sustainability in japan," Evergreen, 2 (1) 49–56 (2015). doi:10.5109/1500427.
4) H. Han, M. Hatta, and H. Rahman, "Smart ventilation for energy conservation in buildings," Evergreen, 6 (1) 44–51 (2019). doi:10.5109/2321005.
5) X. Chen, H. Gao, Z. Tang, W. Dong, A. Li, G. Wang and G. Wang , "Optimization strategies of composite phase change materials for thermal energy storage, transfer, conversion and utilization," Energy & Environmental Science, 13(12), 4498–4535 (2020). doi.org/10.1039/d0ee01355b
6) M. Zeyringer, J. Price, B. Fais, P.-H. Li and E. Sharp ,"Designing low-carbon power systems for Great Britain in 2050 that are robust to the spatiotemporal and inter-annual variability of weather," Nature Energy, 3(5), 395–403(2018). doi.org/10.1038/s41560-018-0128-x
7) J. M. Chen, "Carbon neutrality: Toward a sustainable future," The Innovation, 2(3), 100127 (2021). doi.org/10.1016/j.xinn.2021.100127
8) Benedetti, F., Vogt, M., Elizondo, U.H. Righetti, D., Zimmermann, N. E., & Gruber, N, "Major restructuring of marine plankton assemblages under global warming,". Nature Communications, 12, 5226 (2021). doi.org/10.1038/s41467-021-25385-x
9) Wang, Fang, Jean Damascene Harindintwali, Zhizhang Yuan, Min Wang, Faming Wang, Sheng Li, Zhigang Yin, et al, "Technologies and Perspectives for Achieving Carbon Neutrality," The Innovation 2, no.4,100180(2021).doi.org/10.1016/j.xinn.2021.100180.
10) Mao, Yanpeng, Yibo Gao, Wei Dong, Han Wu, Zhanlong Song, Xiqiang Zhao, Jing Sun, and Wenlong Wang,"Hydrogen Production via a Two-Step Water Splitting Thermochemical Cycle Based on Metal Oxide – A Review," Applied Energy 267,

114860(2020).doi.org/10.1016/j.apenergy.2020.114860.
11) Petkov, Ivalin, and Paolo Gabrielli,"Power-to-Hydrogen as Seasonal Energy Storage: An Uncertainty Analysis for Optimal Design of Low-Carbon Multi-Energy Systems," Applied Energy 274, 115197(2020).doi.org/10.1016/j.apenergy.2020.115197.
12) Roelfsema, Mark, Heleen L. van Soest, Mathijs Harmsen, Detlef P. van Vuuren, Christoph Bertram, Michel den Elzen, Niklas Höhne, et al,"Taking Stock of National Climate Policies to Evaluate Implementation of the Paris Agreement," Nature Communications11,no.1(2020).doi.org/10.1038/s41467-020-15414-6.
13) Rogelj, Joeri, Daniel Huppmann, Volker Krey, Keywan Riahi, Leon Clarke, Matthew Gidden, Zebedee Nicholls, and Malte Meinshausen,"A New Scenario Logic for the Paris Agreement Long-Term Temperature Goal," Nature 573, no. 7774 ,357–63 (2019). doi.org/10.1038/s41586-019-1541-4.
14) D.Bodansky, "The Legal Character of the Paris Agreement," Review of European, Comparative & International Environmental Law, 25(2), 142–150 (2016). https://doi.org/10.1111/reel.12154
15) Bodansky, Daniel, "The Legal Character of the Paris Agreement." Review of European, Comparative & International Environmental Law 25, no. 2, 142–50 (2016). doi.org/10.1111/reel.12154.
16) Ma, Xiaofan, Gang Huang, and Junji Cao,"The Significant Roles of Anthropogenic Aerosols on Surface Temperature under Carbon Neutrality," Science Bulletin 67, no. 5, 470–73 (2022). doi.org/10.1016/j.scib.2021.10.022.
17) Zhang, Xiaoyuan, and Yu Liu,"Circular Economy Is Game-Changing Municipal Wastewater Treatment Technology towards Energy and Carbon Neutrality," Chemical Engineering Journal 429, 132114 (2022). doi.org/10.1016/j.cej.2021.132114.
18) Li, Yinan, Song Lan, Morten Ryberg, Javier Pérez-Ramírez, and Xiaonan Wang,"A Quantitative Roadmap for China towards Carbon Neutrality in 2060 Using Methanol and Ammonia as Energy Carriers," iScience 24, no. 6, 102513 (2021). doi.org/10.1016/j.isci.2021.102513.
19) Chen, Xiao, Piao Cheng, Zhaodi Tang, Xiaoliang Xu, Hongyi Gao, and Ge Wang, "Carbon-Based Composite Phase Change Materials for Thermal Energy Storage, Transfer, and Conversion," Advanced Science 8, no. 9,2001274 (2021). doi.org/10.1002/advs.202001274.
20) Yang, Haiyue, Yushan Liu, Jian Li, Chengyu Wang, and Yudong Li,"Full-Wood Photoluminescent and Photothermic Materials for Thermal Energy Storage," Chemical Engineering Journal 403, 126406 (2021). doi.org/10.1016/j.cej.2020.126406.
21) Shi, Jinming, Mulin Qin, Waseem Aftab, and Ruqiang Zou,"Flexible Phase Change Materials for Thermal Energy Storage," Energy Storage Materials 41,32142(2021).doi.org/10.1016/j.ensm.2021.05.048
22) Abbasi, Mohammad Hosein, Badr Abdullah, Muhammad Waseem Ahmad, Ali Rostami, and Jeff Cullen,"Heat Transition in the European Building Sector: Overview of the Heat Decarbonisation Practices through Heat Pump Technology," Sustainable Energy Technologies and Assessments 48,101630(2021).doi.org/10.1016/j.seta.2021.101630.
23) Kirppu, Heidi, Risto Lahdelma, and Pekka Salminen,"Multicriteria Evaluation of Carbon-Neutral Heat-Only Production Technologies for District Heating," Applied Thermal Engineering 130, 46676(2018).doi.org/10.1016/j.applthermaleng.2017.10.161.
24) https://phys.org/news/2015-12-sun-energy.html#google_vignette
25) https://www.statista.com/statistics/216613/electricity-generated-per-unit-of-fuel-used/
26) Ding, Tianpeng, Yi Zhou, Wei Li Ong, and Ghim Wei Ho,"Hybrid Solar-Driven Interfacial Evaporation Systems: Beyond Water Production towards High Solar Energy Utilization," Materials Today 42, 178–91(2021). doi.org/10.1016/j.mattod.2020.10.022.
27) Quoilin, S., M. Orosz, H. Hemond, and V. Lemort, "Performance and Design Optimization of a Low-Cost Solar Organic Rankine Cycle for Remote Power Generation," Solar Energy 85, no. 5, 955–66 (2011). doi.org/10.1016/j.solener.2011.02.010.
28) Delgado-Torres, Agustín M., and Lourdes García-Rodríguez. "Design Recommendations for Solar Organic Rankine Cycle (ORC)–Powered Reverse Osmosis (RO) Desalination." Renewable and Sustainable Energy Reviews 16, no. 1, 44–53 (2012). doi.org/10.1016/j.rser.2011.07.135.
29) Dunn, Rebecca I., Patrick J. Hearps, and Matthew N. Wright,"Molten-Salt Power Towers: Newly Commercial Concentrating Solar Storage," Proceedings of the IEEE 100, no. 2, 504–15 (2012). doi.org/10.1109/jproc.2011.2163739.
30) Chan, C.W., J. Ling-Chin, and A.P. Roskilly, "A Review of Chemical Heat Pumps, Thermodynamic Cycles and Thermal Energy Storage Technologies for Low Grade Heat Utilisation," Applied Thermal Engineering 50, no. 1, 1257–73 (2013). doi.org/10.1016/j.applthermaleng.2012.06.041.
31) Niedermeier, K., J. Flesch, L. Marocco, and Th. Wetzel,"Assessment of Thermal Energy Storage Options in a Sodium-Based CSP Plant," Applied Thermal Engineering 107, 386–97 (2016). https://doi.org/10.1016/j.applthermaleng.2016.06.152.

32) M. Sharma, R. Dev, "Review and Preliminary Analysis of Organic Rankine Cycle Based on Expander Inled Temperature," Evergreen Joint Journal of Novel Carbon Resource Sciences & Green Asia Strategy, 05 (03) 22–33 (2018). doi:10.5109/1957497.
33) P. Animesh, K. Uddin, K. Thu, B.B. Saha, "Enviromental Assesment and Characteristic of Next Generation Refrigerans" Evergreen Joint Journal of Novel Carbon Resource Sciences & Green Asia Strategy, 04 (04) 8–15 (2018). doi:10.5109/1936218.
34) Zeng, C.L, W Wang, and W.T Wu,"Electrochemical Impedance Models for Molten Salt Corrosion," Corrosion Science 43, no. 4, 787–801 (2001). doi.org/10.1016/s0010-938x(00)00108-6.
35) Lee, Jekyoung, Jeong Ik Lee, Ho Joon Yoon, and Jae Eun Cha, "Supercritical Carbon Dioxide Turbomachinery Design for Water-Cooled Small Modular Reactor Application," Nuclear Engineering and Design 270, 76–89 (2014). doi.org/10.1016/j.nucengdes.2013.12.039.
36) Ahn, Yoonhan, and Jeong Ik Lee,"Study of Various Brayton Cycle Designs for Small Modular Sodium-Cooled Fast Reactor," Nuclear Engineering and Design 276, 128–41 (2014). doi.org/10.1016/j.nucengdes.2014.05.032.
37) Chacartegui, R., J.M. Muñoz de Escalona, D. Sánchez, B. Monje, and T. Sánchez, "Alternative Cycles Based on Carbon Dioxide for Central Receiver Solar Power Plants," Applied Thermal Engineering 31, no. 5, 872–79 (2011). doi.org/10.1016/j.applthermaleng.2010.11.008.
38) Singh, Rajinesh, Sarah A. Miller, Andrew S. Rowlands, and Peter A. Jacobs,"Dynamic Characteristics of a Direct-Heated Supercritical Carbon-Dioxide Brayton Cycle in a Solar Thermal Power Plant," Energy 50, 194–204 (2013). doi.org/10.1016/j.energy.2012.11.029.
39) Turchi, Craig S., Zhiwen Ma, Ty W. Neises, and Michael J. Wagner,"Thermodynamic Study of Advanced Supercritical Carbon Dioxide Power Cycles for Concentrating Solar Power Systems," Journal of Solar Energy Engineering 135, no. 4 (2013). doi.org/10.1115/1.4024030.
40) Turchi, Craig S., Zhiwen Ma, and John Dyreby, "Supercritical Carbon Dioxide Power Cycle Configurations for Use in Concentrating Solar Power Systems," Volume 5: Manufacturing Materials and Metallurgy; Marine; Microturbines and Small Turbomachinery; Supercritical CO2 Power Cycles, June 11, 2012. doi.org/10.1115/gt2012-68932.
41) Garg, Pardeep, Pramod Kumar, and Kandadai Srinivasan,"Supercritical Carbon Dioxide Brayton Cycle for Concentrated Solar Power," The Journal of Supercritical Fluids 76, 54–60(2013). doi.org/10.1016/j.supflu.2013.01.010.
42) Besarati, Saeb M., and D. Yogi Goswami, "Analysis of Advanced Supercritical Carbon Dioxide Power Cycles with a Bottoming Cycle for Concentrating Solar Power Applications," Journal of Solar Energy Engineering 136, no. 1 (2013). doi.org/10.1115/1.4025700.
43) Rahman, Shek, Zafar Said, and Salah Issa, "Performance Evaluation and Life Cycle Analysis of New Solar Thermal Absorption Air Conditioning System," Energy Reports 6 (February 2020): 673–79. doi.org/10.1016/j.egyr.2019.11.136.
44) Muneer, T., and A.H. Uppal, "Modelling and Simulation of a Solar Absorption Cooling System," Applied Energy 19, no. 3, 209–29 (1985). doi.org/10.1016/0306-2619(85)90009-1.
45) Li, Z.F, and K Sumathy, "Technology Development in the Solar Absorption Air-Conditioning Systems," Renewable and Sustainable Energy Reviews 4, no. 3, 267–93(2000).doi.org/10.1016/s1364-0321(99)00016-7.
46) M.I. Alhamid, S. Bismo, I.T. Ramadhan, A. Yatim, "Study on The Effectiveness of Ozonation Technique in Preventing Scale Precipitation on Closed System Cooling Towers," Evergreen Joint Journal of Novel Carbon Resource Sciences & Green Asia Strategy, 06 (01), 65–70 (2019). doi:10.5109/2321013
47) Sokhansefat, T., D. Mohammadi, A. Kasaeian, and A.R. Mahmoudi,"Simulation and Parametric Study of a 5-Ton Solar Absorption Cooling System in Tehran," Energy Conversion and Management 148, 339–51 (2017). doi.org/10.1016/j.enconman.2017.05.070.
48) Shukla, Anoop Kumar, Achintya Sharma, Meeta Sharma, and Gopal Nandan, "Thermodynamic Investigation of Solar Energy-Based Triple Combined Power Cycle," Energy Sources, Part A: Recovery, Utilization, and Environmental Effects 41, no.10,1161–79(2018).doi.org/10.1080/15567036.2018.1544995.
49) Khandelwal, Neelam, Meeta Sharma, Onkar Singh, and Anoop Kumar Shukla,"Recent Developments in Integrated Solar Combined Cycle Power Plants," Journal of Thermal Science 29, no. 2, 298–322 (2020). doi.org/10.1007/s11630-020-1278-2.
50) Sharma, Achintya, Anoop Kumar Shukla, Onkar Singh, and Meeta Sharma,"Recent Advances in Gas/Steam Power Cycles for Concentrating Solar Power," International Journal of Ambient Energy 43, no.1,4716–27(2021).doi.org/10.1080/01430750.2021.1919552.
51) Sharma, Meeta, Anoop Kumar Shukla, Akash Singh, Sukrit Johri, and Harsh Pratap Singh ,"Parametric Analysis of Solar Energy Conversion System Using Parabolic Concentrator and Thermopile," International Journal of Ambient Energy 41, no. 12, 1409-14(2018).doi.org/10.1080/01430750.2018.1517672.

52) M.A. Islam, P.Animesh, K Thu, B.B. Saha, "Study on Performance and Environmental Impact of Supermarket Refrigeration System in Japan," Evergreen Joint Journal of Novel Carbon Resource Sciences & Green Asia Strategy, 06 (02), 168–176(2019). doi:10.5109/2321014.
53) Khan, Razzak, Anoop Kumar Shukla, Meeta Sharma, Rakesh Kumar Phanden, and Shivam Mishra, "Thermodynamic Investigation of Intercooled Reheat Gas Turbine Combined Cycle with Carbon Capture and Methanation," Materials Today: Proceedings 38,449-55(2021).doi.org/10.1016/j.matpr.2020.07.680.
54) Sharma, Achintya, Meeta Sharma, Anoop Kumar Shukla, and Nitin Negi, "Evaluation of Heat Recovery Steam Generator for Gas/Steam Combined Cycle Power Plants," Lecture Notes in Mechanical Engineering,189–200(2019).doi.org/10.1007/978-981-13-6416-7_18.
55) Shukla, Anoop Kumar, and Onkar Singh, "Thermodynamic Investigation of Parameters Affecting the Execution of Steam Injected Cooled Gas Turbine Based Combined Cycle Power Plant with Vapor Absorption Inlet Air Cooling," Applied Thermal Engineering 122, 380–88 (2017). doi.org/10.1016/j.applthermaleng.2017.05.034.
56) Sachdeva, Jatin, and Onkar Singh, "Thermodynamic Analysis of Solar Powered Triple Combined Brayton, Rankine and Organic Rankine Cycle for Carbon Free Power," Renewable Energy 139, 765–80 (2019). doi.org/10.1016/j.renene.2019.02.128.
57) Singh, Ragini, and Onkar Singh,"Comparative Study of Combined Solid Oxide Fuel Cell-Gas Turbine-Organic Rankine Cycle for Different Working Fluid in Bottoming Cycle," Energy Conversion and Management 171, 659–70, (2018). doi.org/10.1016/j.enconman.2018.06.009.
58) Singh, Onkar, Gaitry Arora, and Vinod Kumar Sharma, "Energy-Exergy Analysis of Solarized Triple Combined Cycle Having Intercooling, Reheating and Waste Heat Utilization," Tecnica Italiana-Italian Journal of Engineering Science 65, no. 1, 93–104 (2021).doi.org/10.18280/ti-ijes.650114.
59) Kanaujiya, Amit, and Onkar Singh, "Thermodynamic Study for Performance Enhancement of Supercritical Carbon Dioxide Cycle," Lecture Notes in Mechanical Engineering,417–33 (2021). doi.org/10.1007/978-981-16-3497-0_33.
60) Masood, G. M., and Onkar Singh, "Thermodynamic Investigations on PDC Based Solar Air Conditioning System," Journal of Physics: Conference Series 2178, no. 1, 012023(2022). doi.org/10.1088/1742-6596/2178/1/012023.
61) Khaliq, Abdul, "Exergy Analysis of Gas Turbine Trigeneration System for Combined Production of Power Heat and Refrigeration," International Journal of Refrigeration 32, no. 3,534–45 (2009). https://doi.org/10.1016/j.ijrefrig.2008.06.007.
62) Dostal Vaclav, "Supercritical carbon dioxide for next generation nuclear reactors," Doctor of science,(2004), Massachusetts Institute of Technology.https:hdl.handle.net/1721.1/67671.
63) Wei, Lili, Zhenjun Ma, Xuemei Gong, and Xiujuan Guo,"Experimental Investigation and Performance Analysis of an Organic Rankine Cycle for Low-Temperature Heat to Electricity Generation," International Journal of Low-Carbon Technologies 14,no.4,500–507(2019).doi.org/10.1093/ijlct/ctz037.
64) Kilic, Muhsin, and Omer Kaynakli,"Second Law-Based Thermodynamic Analysis of Water-Lithium Bromide Absorption Refrigeration System," Energy 32,no.8,1505-12(2007).doi.org/10.1016/j.energy.2006.09.003.
65) https://www.nist.gov/srd/refprop
66) https://fchartsoftware.com/ees/
67) Raghuwanshi ,Satish and Laad Piyush, "Analysis of Lithium Bromide-Water (LiBr- H2O) Vapour Absorption Refrigeration System Using First Law of Thermodynamics," Proceedings of Recent Advances in Interdisciplinary Trends in Engineering & Applications (RAITEA) 2019. doi.org/10.2139/ssrn.3351049
68) Mohamed S. Shahina, Mehmet F. Orhana and Faruk Uygul, "Thermodynamic analysis of parabolic trough and heliostat field solar collectors integrated with a Rankine cycle for cogeneration of electricity and heat,"SolarEnergy,136,183–196,(2016). doi.org/10.1016/j.solener.2016.06.057